P1.30

THE ANNUAL CYCLE OF EARTH RADIATION BUDGET FROM CLOUDS AND THE EARTH'S RADIANT ENERGY SYSTEM (CERES) DATA

Pamela E. Mlynczak*
Science Systems and Applications, Inc., Hampton, VA

G. Louis Smith
National Institute of Aerospace, Hampton, VA

ABSTRACT

The annual cycle of Earth radiation budget is investigated by use of data from the Clouds and Earth Radiant Energy System (CERES). Monthly-mean maps of reflected solar flux and Earth-emitted flux on a 1^{o} grid are used for the study. The annual cycles of absorbed solar radiation, Earth-emitted radiation and net radiation are described by use of principal components for the time variations, for which the corresponding geographic variations are the empirical orthogonal functions. The Earth's surface is partitioned into land and ocean for the analysis.

1. INTRODUCTION

The annual cycle of Earth radiation budget is the response of the climate system to the annual cycle of solar input. Examining the response of a system to a cyclical forcing is an important method for understanding the dynamics of the system. The absorbed insolation depends on the albedo, which is a dynamic quantity depending largely on the movement of major cloud systems as they interact with the solar heating and other parts of the climate system. Snow and ice cover also affect the albedo to provide a forcing of the absorbed flux of energy. The temperatures of the land, atmosphere and ocean vary in response to the cyclic heating and together with the clouds cause the longwave flux at the top of the atmosphere to vary. The geographical distribution of fluxes and their time variations are fundamental aspects of climate, as these radiation fluxes create the temperature distributions that drive the atmospheric and oceanic circulations.

The annual cycle of ASR is driven by the cycle of solar declination and modulated by clouds and snow and ice cover. The OLR and net radiation are responses to the ASR cycle as affected by the heat storage and transport. Knowledge of the annual cycles of OLR and net radiation thus provide much information about these processes.

This paper presents a study that used data from the Clouds and the Earth's Radiant Energy System (CERES) to investigate the annual cycle of radiation. Monthly-mean maps of reflected solar flux and Earth-emitted flux on a 1^{o} grid were used for the study. The absorbed solar radiation is computed from the CERES data by subtracting the reflected flux from the insolation at the top of the atmosphere. The annual cycles of absorbed solar radiation and Earth-emitted radiation fluxes are described by use of principal components for the time variations, for which the corresponding geographic variations are the empirical orthogonal functions. The principal components provide the most concise quantitative description of the data and are a set of basis functions for quantitative comparisons of observed fluxes with those computed by models. The immense heat capacity of the ocean causes it to have a slow response to the annual cycle of heating relative to land, and the atmosphere is closely coupled with the surface, so the Earth's surface is partitioned into land and ocean for the analysis.

Earlier studies of the annual cycle of Earth-emitted radiation budget (Bess et al. 1992) and absorbed solar radiation (Smith et al. 1990) used wide-field-of-view data from the Earth Radiation Budget instrument aboard the Nimbus 6 and 7 spacecrafts (Smith et al. 1977; Jacobowitz et al. 1984). The resolution, even after being enhanced (Smith and Green 1981; Smith and Rutan 1990), was 15 degrees in latitude and at the equator was 15 degrees in longitude. Consequently the Intertropical Convergence Zone (ITCZ) and its movements could hardly be detected. The CERES data set provides the resolution needed to see these changes.

2. DATA AND ANALYSIS METHOD

The CERES_SYN1deg-month-lite_Terra_Ed2.5-Beta product used for this study was provided by the CERES project (Wielicki et al. 1996) and currently contains monthly mean values at the top of atmosphere (TOA) from March 2000 through December 2008. (The data set is available at http://ceres.larc.nasa.gov.) The Edition2.5 is an improvement over Edition2 CERES products since all known instrument calibration artifacts, such as spectral darkening in the SW instrument, were removed over the Terra CERES record. The SYN-lite product uses improved Angular Directional Models (ADMs) to convert the radiances into fluxes and is an improvement over the ERBElike product, which uses the traditional ERBE algorithms (Wielicki et al. 1998). The ADMs used are selected based on scene type and viewing geometry (Loeb et al. 2005, 2007), and MODIS cloud properties help identify the scene types. To derive the daily mean fluxes, the SYN-lite product uses geostationary derived fluxes and cloud properties to estimate the diurnal signal in between the Terra (10:30LT) CERES flux measurements. The geostationary fluxes have been carefully normalized to the CERES fluxes in order to maintain the CERES

Corresponding author address:
Pamela E. Mlynczak, SSAI, 1 Enterprise Parkway, Suite 200, Hampton, VA 23666.
E-mail: Pamela.E.Mlynczak@nasa.gov

calibration in the flux product. Not accounting for the diurnal cycle could cause up to a 30 W m^{-2} 1° regional bias over maritime stratus and land afternoon convection areas. The SYN-lite product is a limited parameter product and is a precursor of the Edition3 CERES products to be completed by early 2011.

The SYN-lite data set used for this analysis has 64800 1°x1° equal angle regions, with monthly mean values of top of atmosphere (TOA) reflected shortwave, outgoing longwave (OLR) and net fluxes as well as insolation and albedo. Absorbed shortwave radiation (ASR) must be calculated. The reflected shortwave flux contains a twilight flux correction (Kato and Loeb 2003), but the net flux does not, so to gain consistency in the fluxes studied, ASR is calculated as the product of the insolation and (1.0 – albedo), thereby removing the twilight flux correction. This effect is on the order of 1 W m^{-2} or less locally. The climatological monthly means for each calendar month are computed for the period March 2000 through December 2008, which includes 106 months. The climatological annual mean over the period is then formed from the climatological monthly means. For any given region, the annual cycle is calculated by taking the difference between that region's 12 climatological monthly mean values and the climatological annual mean.

In order to quantify the annual cycle for all 64800 regions, principal component analysis is used. The first step is to form a covariance matrix as

$$\Gamma(m,m') = \sum_{x=1}^{64800} w(x)V(x,m)V(x,m'),$$

where $V(x,m)$ denotes the annual cycle at region x for month m and $w(x)$ is the area weighting for region x. Since there are 12 monthly means in this study, the covariance matrix is 12x12. The principal components of this covariance matrix Γ are the eigenvectors $PC_n(m)$ where $n \in [1,12]$. They describe the temporal pattern in the annual cycle, and the eigenvalues λ_n represent the variance explained by each PC. For each flux, the 12 PCs are projected onto the 12 climatological monthly mean maps to obtain the empirical orthogonal functions $EOF_n(x)$, giving the spatial coefficients associated with each PC. Thus the annual cycle of a flux at region x and month m can be represented by

$$V(x,m) = \sum_{n=1}^{12} \mathrm{PC}_n(m)\mathrm{EOF}_n(x).$$

3. GLOBAL TIME AND SPACE VARIATIONS

3.1 Annual Mean Maps of TOA Fluxes

The global annual mean ASR is 242.8 W m^{-2}, and Figure 1a shows the geographical distribution of this mean. The dominant feature is the zonal variation due to insolation at TOA, but the longitudinal variations over ocean are due to clouds. In general, the mean ASR is highest over the oceans, which have low albedos. Subsidence areas near the equator have large values because of the lack of clouds. The high ASR over the equatorial Pacific Ocean and the west equatorial Indian Ocean also indicates the paucity of cloud over these regions. A strip of lower values just north of the equator indicates the Intertropical Convergence Zone (ITCZ) and its associated cloudiness. At the equator, the convective regions of the Amazon Basin, the Congo Basin, and the Maritime Continent are low compared to the rest of the zone. The deserts of North Africa and the Middle East have low annual mean ASR compared to the rest of that latitudinal zone because of their high albedos. Greenland also has a high albedo due to its ice/snow cover, which is apparent in its lower ASR values.

Figure 1b is a map of the annual mean outgoing longwave radiation, and the global annual mean is 238.8 W m^{-2}. Like the annual mean ASR, the main pattern is zonal in the extratropics, but cloud effects are prominent elsewhere. The cold cloud tops in the ITCZ reduce OLR just above the equator. The subsidence zones of the oceans and deserts have the greatest annual mean OLR. As with annual mean ASR, the three convective regions over South America, the Congo, and the Maritime Continent have local minima of annual mean OLR in their zones. Although the Greenland Plateau has the lowest annual mean OLR in the Northern Hemisphere, Antarctica has even lower values.

Figure 1c is a map of the annual mean net radiation, and its global mean is 4.0 W m^{-2}. The global net balance has been recognized as being a measure of the error in the system, which in this case includes errors in measurements, modeling of the ADMs, and temporal and spatial interpolation. Our concern in this study is the variability of the annual cycle in space and time; therefore the imbalance indicated by the global annual mean net radiation will not be addressed here. A CERES data product has been created where the fluxes are more in balance (Loeb et al. 2009). Since the mean net flux is the difference between the mean ASR and the mean OLR, it is strongly zonal as well, with longitudinal differences due to variations in clouds. The mean net flux is negative over the North African and Middle Eastern deserts, showing net cooling in these subsidence regions (Charney, 1975). The mean net flux over the Australian desert is also lower than its zonal mean, although the contrast is not as large as over the Northern Hemisphere deserts. Off the west coasts of South America and southern Africa, the mean net flux has features that are likely due to low-level maritime cloudiness. The annual mean net goes from a surplus to a deficit at 40° latitude in each hemisphere.

3.2 Root Mean Square of Annual Cycles

RMS, W m^{-2}	ASR	OLR	Net
Land	73.4	21.3	62.0
Ocean	73.8	12.1	69.8

Table 1. Root mean square of the annual cycles of absorbed shortwave radiation, outgoing longwave radiation, and net radiation over land and ocean in W m^{-2}.

Over land, the annual cycle of ASR has a RMS of 73.4 W m^{-2}, as shown in Table 1. This value is a measure of the amplitude of the cycle. In the absence of storage or transport of heat, OLR would equal ASR locally and instantaneously, so that the RMS of the OLR annual cycle would equal that of ASR, and the RMS of the net radiation annual cycle would be very small. However, the RMS values in Table 1 show that this is not the case. Given strong transport, surplus heat in low latitudes is quickly moved to high latitudes and therefore becomes part of the annual mean, flattening the annual mean map of OLR and causing the annual cycle of OLR to be smaller (21.2 W m^{-2}) than that of ASR. With a small cycle of OLR, the net radiation annual cycle would then be close to the ASR cycle. The RMS values of the net and OLR cycles are thus a measure of the transport of heat.

For ocean, the storage of heat is large and the cycles of surface temperature and therefore OLR are small. The annual cycle of OLR has a RMS of 12.0 W m^{-2} (Table 1). Consequently, the annual cycle of net radiation is close to that of ASR, and here the difference is only 4 W m^{-2}. The heat transport is also large in the ocean, but the relative small size of the OLR cycle can be explained simply by the heat storage. It remains to partition the effects of storage and transport of heat.

3.3 Principal Component Analysis of ASR

Table 2 shows the first four eigenvalues of the annual cycle of ASR. These normalized eigenvalues are very similar for land and ocean. The first PC describes about 96% of the variability of the ASR, and thus PC-1 explains most of the annual cycle of ASR for both land and ocean. The second PC describes 2-3%, leaving little other variation to be described by higher order terms.

ASR		
Eigenvalues	Land	Ocean
1	.958	.963
2	.028	.022
3	.008	.009
4	.003	.003
Sum, 1 through 4	.997	.997

Table 2. The normalized eigenvalues of, or fraction of variance explained by, the first four PCs of the annual cycle of absorbed shortwave radiation.

Figure 2 shows the first three principal components of the annual cycle of ASR over land and ocean as a function of month of the year. PC-1 for land (Fig. 2a) is very sinusoidal in shape with an amplitude of 100 W m^{-2} and a peak in June. Because it describes nearly 96% of the variance, it represents the annual cycle of ASR. PC-2 is a wavenumber 2 with maxima of about 18 W m^{-2} near the solstices and minima of -18 W m^{-2} near the equinoxes. It represents a semiannual cycle. These first two PCs behave similarly to the annual cycle of insolation as described with principal components by Wilber et al. (2006). The insolation varies with solar declination angle, and most of its variation is sinusoidal except in the polar regions, where the extended zero values of polar night require a second term to describe them, namely PC-2. PC-3 is a wavenumber 1 sine, out of phase with PC-1, and it has an amplitude of about 6 W m^{-2}. It is due to cloud and snow effects that lag the solar declination. The first three PCs for ASR over ocean (Fig. 2b) are very similar to those for land.

The geographical distribution of coefficients that corresponds to PC-1 for ASR over land is EOF-1, shown in Figure 3a. EOF-1 is nearly zonal, with values ranging from nearly 2 at high northern latitudes to nearly -2 at high southern latitudes, except across Eurasia, which has a more complex variation with longitude. The positive EOF-1 values of the Northern Hemisphere, when multiplied by PC-1, show an increase in ASR from March through September. Conversely, the negative values of EOF-1 in the Southern Hemisphere show an increase there in ASR from September through March. This is exactly what is expected, since PC-1 explains over 95% of the annual cycle of ASR, which is mainly a representation of the changing insolation throughout the year. EOF-1 is small near the equator since insolation there does not vary as much as at higher latitudes. The Greenland plateau and Antarctica have smaller variations of ASR because of their high albedo. EOF-1 for ASR over ocean is shown in Fig. 3b. It displays the same zonal structure that EOF-1 for land does. The longitudinal variations in the tropics for the annual mean are not seen here.

Figure 4a shows the EOF-2 of ASR over land. EOF-2 represents the coefficients of the semiannual PC-2, which explains only 2.8% of the annual cycle. Values between 60°N and 60°S are generally small. Larger positive values at high latitudes show that there is more absorption of shortwave during the summer months and that ASR goes to zero in the winter months. EOF-2 has local minima over Central America, equatorial Africa, and southern Asia, indicating a reduction in ASR during June and July, the time of the monsoons. EOF-2 over ocean (Fig. 4b) shows the same zonal structure as EOF-2 over land. The Bermuda/Azores High shows over the North Atlantic. The dark green bands near the equator indicate the north-south motions of the ITCZ throughout the year. Movements of the associated subsidence zones can also be seen.

3.4 Principal Component Analysis of OLR

OLR is the response of the surface and atmosphere to ASR; therefore, it is expected that similarities will exist in the principal components and EOFs of the annual cycles of the two fluxes. Table 3 shows that the first eigenvalues of the annual cycle of OLR are 0.88 for land and 0.79 for ocean. These values indicate that the first PC strongly dominates and describes most of the annual cycle.

OLR		
Eigenvalues	Land	Ocean
1	.882	.786
2	.054	.086
3	.031	.048
4	.015	.035
Sum, 1 through 4	.982	.955

Table 3. The normalized eigenvalues of, or fraction of variance explained by, the first four PCs of the annual cycle of outgoing longwave radiation.

Figure 5a shows the first three PCs of the annual cycle of OLR over land. Like PC-1 for ASR, PC-1 for OLR is sinusoidal in shape and is an annual cycle. Its amplitude is smaller, about 27 W m^{-2}, and it has a maximum in July and a minimum in January, so that it lags the PC-1 for ASR by a month. PC-1 for the annual cycle of OLR over ocean is shown in Fig. 5b. Its shape is similar to PC-1 for land, but its amplitude is smaller, 15 W m^{-2}.

For ASR, the principal components of any given order for both land and ocean are nearly identical. For OLR, however, this is not the case. PC-2 of OLR over land is similar to PC-3 of OLR over ocean. Both are wavenumber 2 and represent the semiannual cycle, as does PC-2 of ASR. These PCs explain about 5% of the variance in the OLR annual cycle. They have local maxima in January and July/August, but the minima in PC-3 over ocean lag those in PC-2 over land by one-half to one month. PC-3 over land and PC-2 over ocean are similar. Both are a wavenumber 1 out of phase with PC-1, lagging by three months, and they have amplitudes of about 6 W m^{-2}.

Figure 6a shows EOF-1 of OLR over land, the geographical distribution of coefficients corresponding to PC-1. This map and the map of EOF-1 over ocean (Fig. 6b) show a generally zonal pattern in the extratropics that is a function of the sine of the latitude, similar to that of EOF-1 of ASR (Fig. 3), with high positive values over northern latitudes and high negative values over southern latitudes. In the tropics, however, the movement of deep convective centers (from the Congo Basin to equatorial Africa, for example) dominates EOF-1 over land and is shown by negative to positive bands across the equator. These same bands are also found in EOF-1 over ocean and indicate the north-south movements of cloud systems and the associated subsidence zones as they follow the sun. For example, note the dark blue areas over India and the surrounding ocean. These negative EOF-1 values when multiplied with PC-1 show that OLR is reduced during the summer monsoon season, as one would expect with cold convective cloud tops.

EOF-2 for land and EOF-3 for ocean corresponding to the semiannual cycle of OLR are shown in Figure 7. Most of the variation over land and ocean occurs from 30°N to 30°S. The negative to positive to negative bands can be clearly seen over Africa and over the Indian Ocean. This pattern represents the north-south movements of clouds throughout the year.

3.5 Principal Component Analysis of Net Radiation

Like ASR, the eigenvalues of the annual cycle of net radiation show that the first principal components for both land and ocean explain more than 95% of the variability in the cycle (Table 4). PC-2 describes 2-3% as well, just like those of ASR.

Net		
Eigenvalues	Land	Ocean
1	.953	.969
2	.031	.022
3	.009	.006
4	.004	.002
Sum, 1 through 4	.997	.999

Table 4. The normalized eigenvalues of, or fraction of variance explained by, the first four PCs of the annual cycle of net radiation.

The first three PCs of the annual cycle of net flux over land are shown in Fig. 8a. PC-1 is sinusoidal in nature, matching the temporal pattern of PC-1 for ASR over land. The amplitude is somewhat smaller, since for net flux, OLR is subtracted from ASR. The next two PCs represent the semiannual cycle and the out-of-phase annual cycle, respectively, and these are in phase with those for ASR. Since the second and third eigenvalues are so small, PC-2 and PC-3 account for very little of the variation of the annual cycle, and they are nearly identical to those of ASR. The PCs over ocean are shown in Fig. 8b and are very similar to those for ASR because the OLR has a small RMS compared to ASR. PC-1 over ocean has a slightly larger cycle of net radiation than over land since its cycle of OLR is smaller.

EOF-1 for the net flux over land is shown in Fig. 9a. The pattern is nearly zonal, just like that of EOF-1 for ASR. Figure 9b shows EOF-1 over ocean, which is also zonal and corresponds well with EOF-1 over land. Some deviations from the zonal pattern can be seen near the west coasts of North America, South America, and southern Africa. The EOF-2 maps over land and ocean that correspond to the semiannual cycle are shown in Fig. 10. These are also nearly the same as those for ASR.

4. CONCLUSION

The first principal component describes a large majority of the variance in the annual cycle of the absorbed solar radiation, Earth-emitted radiation and the net radiation fluxes. This conciseness of the description makes the principal component useful as a method for comparing observed radiation budget with that computed by a model. The magnitude of the Earth-emitted radiation and its time lag relative to that of the absorbed solar radiation are important descriptors of the climate system and are computed for the first principal components.

5. ACKNOWLEDGEMENTS

The authors gratefully acknowledge support by the CERES program from the NASA Science Mission Directorate through Langley Research Center to Science Systems and Applications Inc. and to the National Institute of Aerospace. They also acknowledge the CERES project at NASA Langley for access to the data set.

6. REFERENCES

Bess, T. D., G. L. Smith, T. P. Charlock, and F. G. Rose, 1992: Annual and interannual variations of Earth-emitted radiation based on a 10-year data set. *J. Geophys. Res.*, **97D**, 12825-12835.

Charney, J. G., 1975: Dynamics of deserts and drought in the Sahel. *Quart. J. Roy. Meteor. Soc.*, **101**, 193-202.

Jacobowitz, H., H. V. Soule, H. L. Kyle, F. B. House, and the NIMBUS 7 ERB Experiment Team, 1984.The Earth radiation budget (ERB) experiment: An overview. *J. Geophys. Res*., **89D,** 5021-5038.

Kato, S., and N. G. Loeb, 2003: Twilight irradiance reflected by the earth estimated from Clouds and the Earth's Radiant Energy System (CERES) measurements. *J. Climate*, **16**, 2646-2650.

Loeb, N. G., S. Kato, K. Loukachine, and N. M. Smith, 2005: Angular distribution models for top-of-atmosphere radiative flux estimation from the Clouds and the Earth's Radiant Energy System instrument on the Terra satellite. Part I: Methodology, *J. Atmos. Oceanic Technol.*, **22**, 338-351.

Loeb, N. G., S. Kato, K. Loukachine, N. M. Smith, and D. R. Doelling, 2007: Angular distribution models for top-of-atmosphere radiative flux estimation from the Clouds and the Earth's Radiant Energy System instrument on the Terra satellite. Part II: Validation, *J. Atmos. Oceanic Technol.*, **24**, 564-584.

Loeb, N. G., and Coauthors, 2009: Towards optimal closure of the Earth’s top-of-atmosphere radiation budget. *J. Climate*, **22**, 748-766.

Smith, G. L., and R. N. Green, 1981: Deconvolution of wide-field-of-view radiometer measurements of earth-emitted radiation, Part I: Theory. *J. Atmos. Sci.*, **38**, 461-473.

Smith, G. L., and D. Rutan, 1990: Deconvolution of wide-field-of-view measurements of reflected solar radiation. *J. Appl. Meteor.,* **29**, 109-122.

Smith, G. L., D. Rutan, T. P. Charlock, and T. D. Bess, 1990: Annual and interannual variations of absorbed solar radiation based on a 10-year data set. *J. Geophys. Res.*, **95D**, 16639-16652.

Smith, W. L., J. Hickey, H. B. Howell, H. Jacobowitz, D. T. Hilleary, and A. J. Drummond, 1977: Nimbus-6 earth radiation budget experiment. *Appl. Opt*., **16**, 306-318.

Wielicki, B. A., B. R. Barkstrom, E. F. Harrison, R. B. Lee III, G. L. Smith, and J. E. Cooper, 1996: Clouds and the Earth's Radiant Energy System (CERES): An Earth Observing System Experiment. *Bull. Amer. Meteor. Soc.*, **77**, 853-868.

Wielicki, B. A., and Coauthors, 1998: Clouds and the Earth’s Radiant Energy System (CERES): Algorithm overview. *IEEE Trans. Geosci. Remote Sens.*, **36**, 1127-1141.

Wilber, A. C., G. L. Smith, S. K. Gupta, and P. W. Stackhouse, 2006: Annual cycles of surface shortwave radiative fluxes. *J. Climate*, **19**, 535-547.

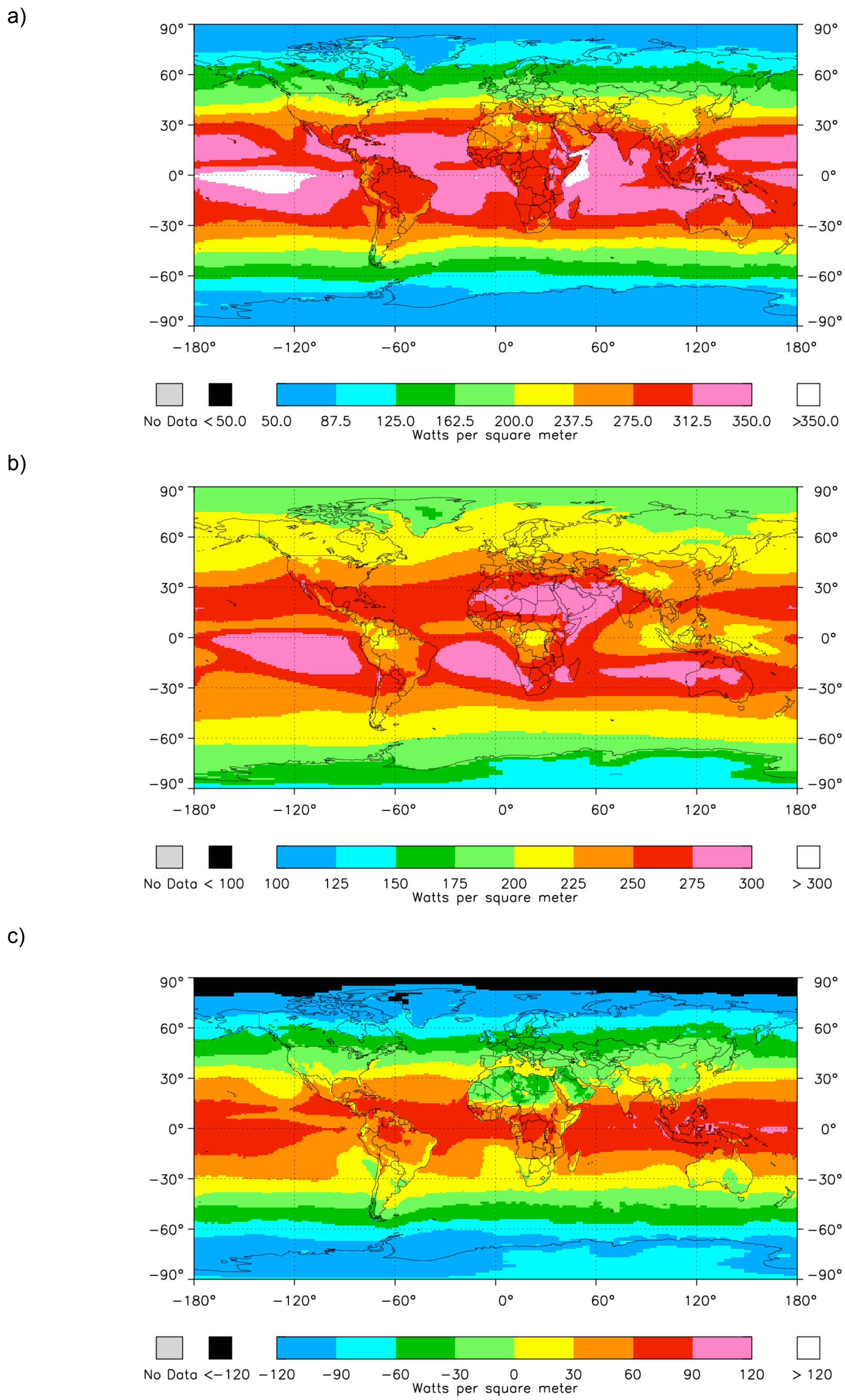

Figure 1. Annual mean maps of a) ASR, b) OLR, and c) net radiation.

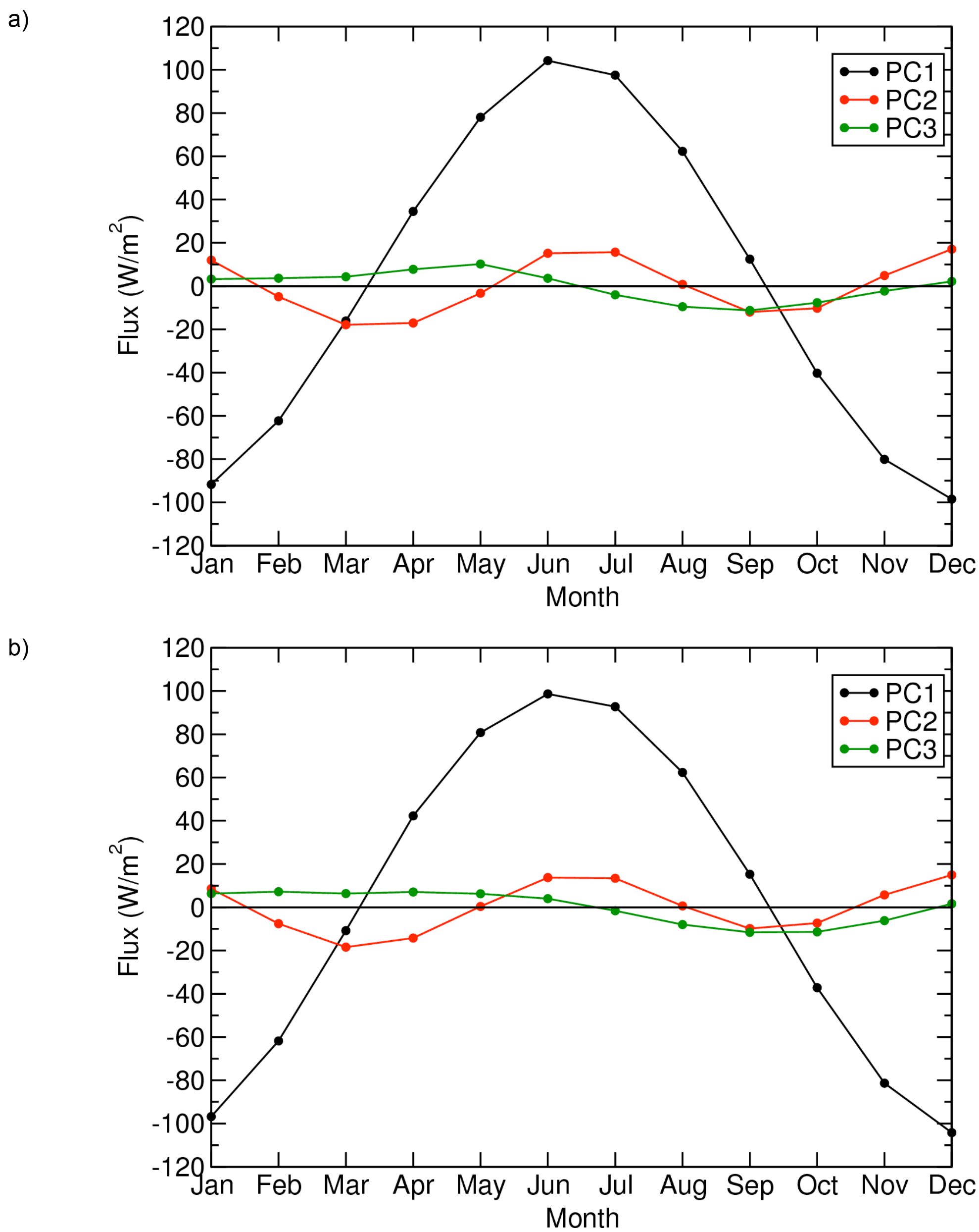

Figure 2. PCs of ASR over a) land and b) ocean.

a)

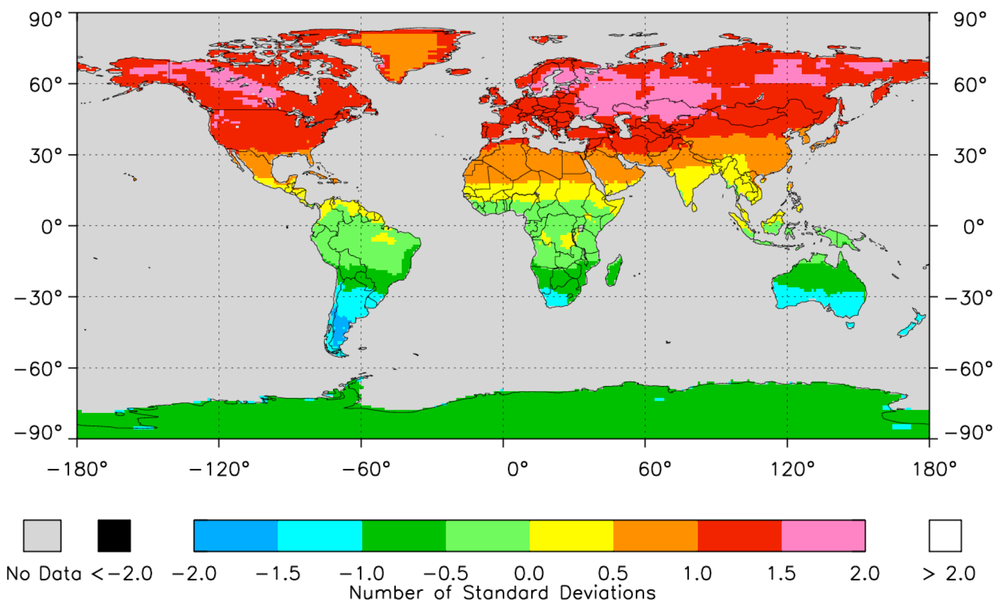

b)

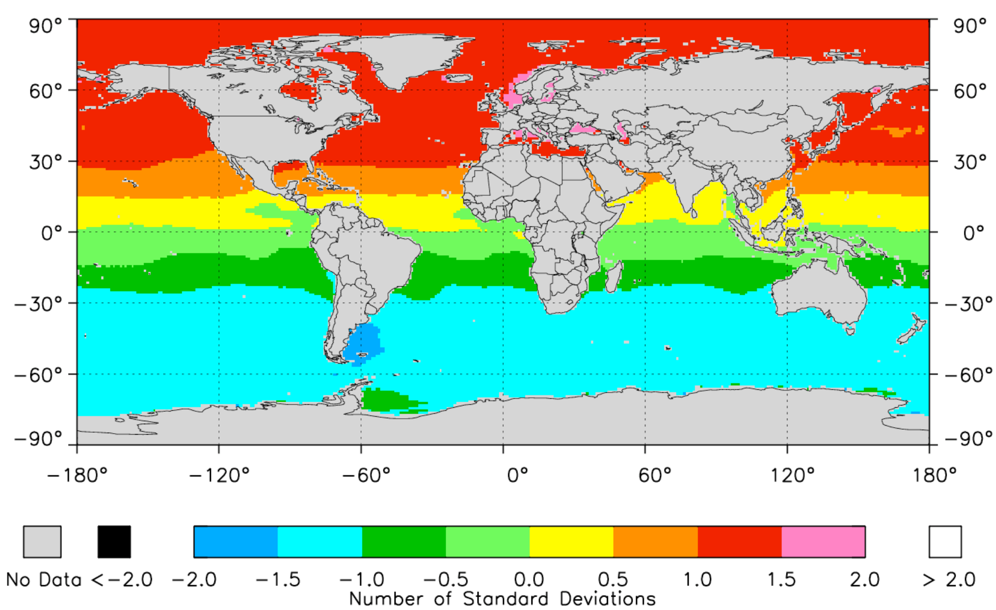

Figure 3. EOF-1 for ASR over a) land and b) ocean.

a)

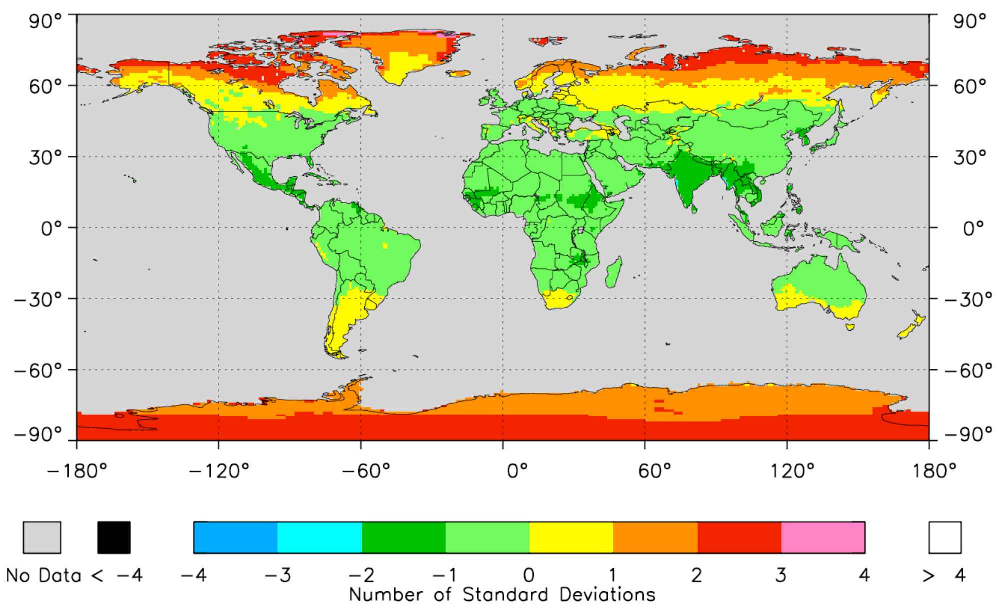

b)

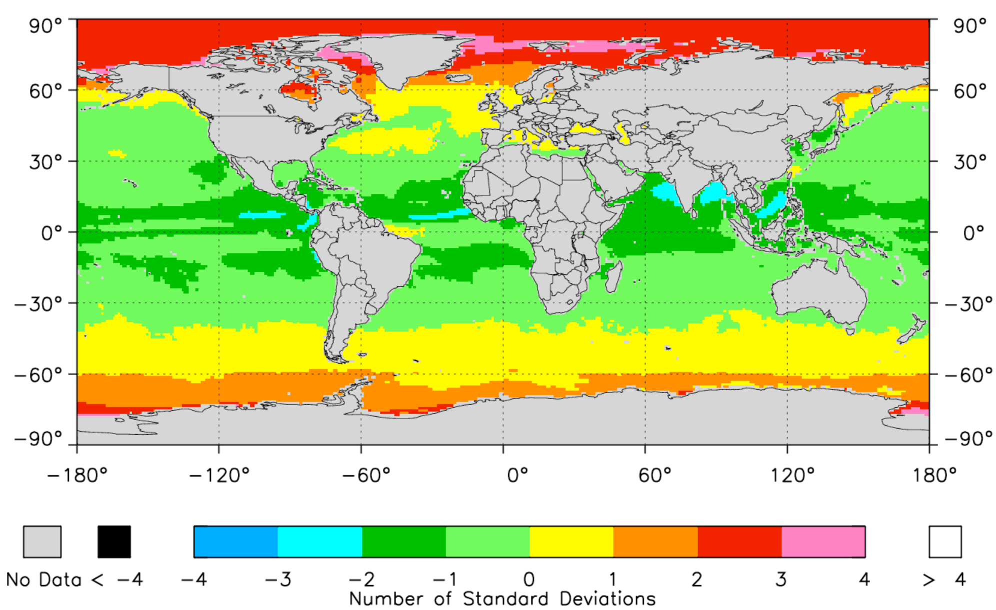

Figure 4. EOF-2 for ASR over a) land and b) ocean.

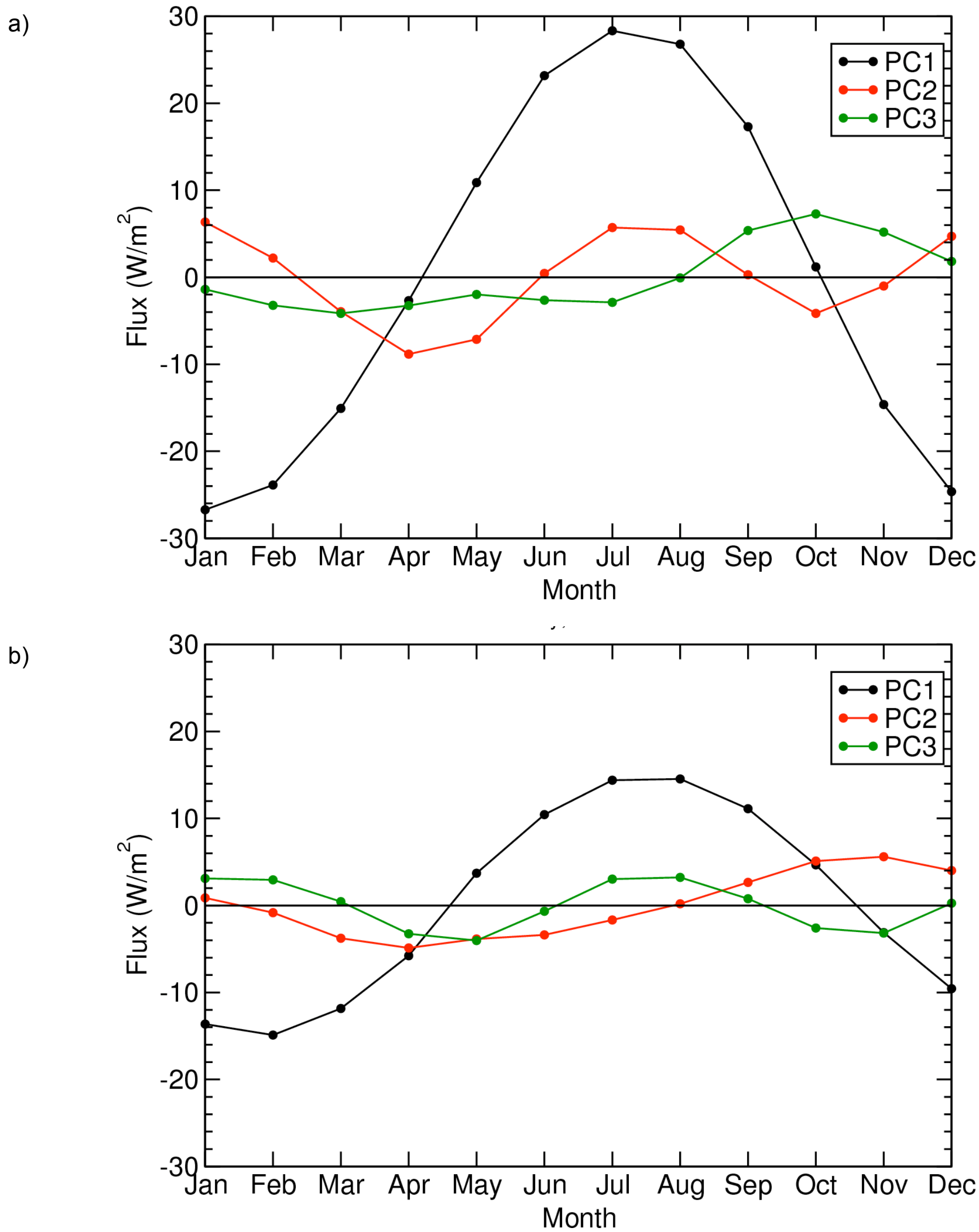

Figure 5. PCs of OLR over a) land and b) ocean.

a)

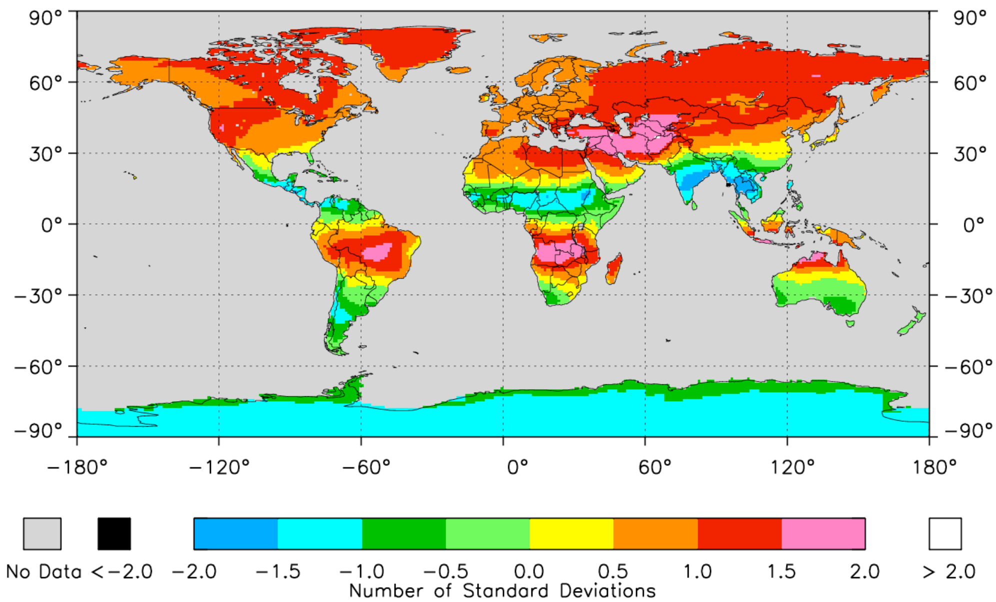

b)

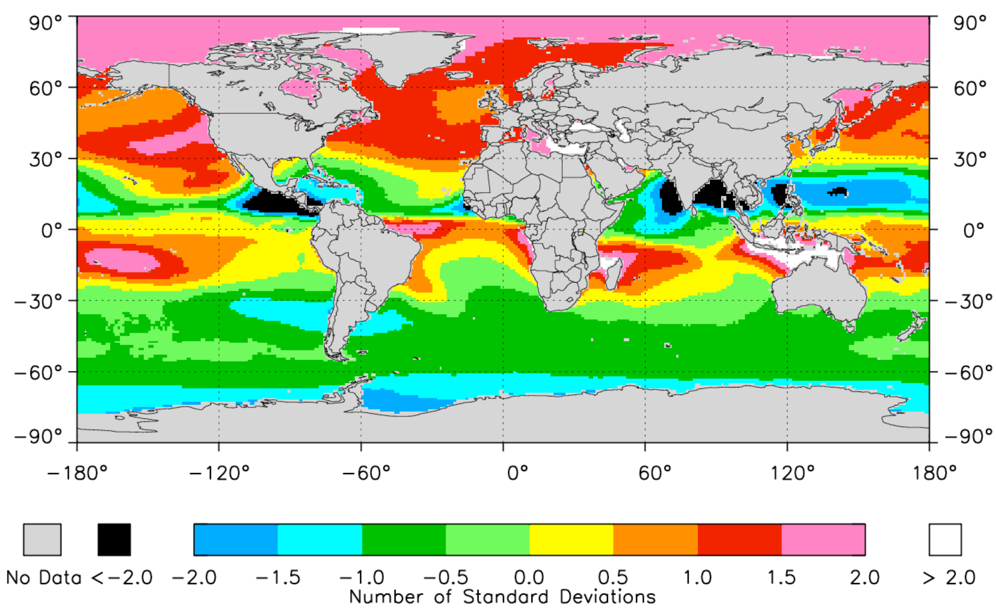

Figure 6. EOF-1 of OLR over a) land and b) ocean.

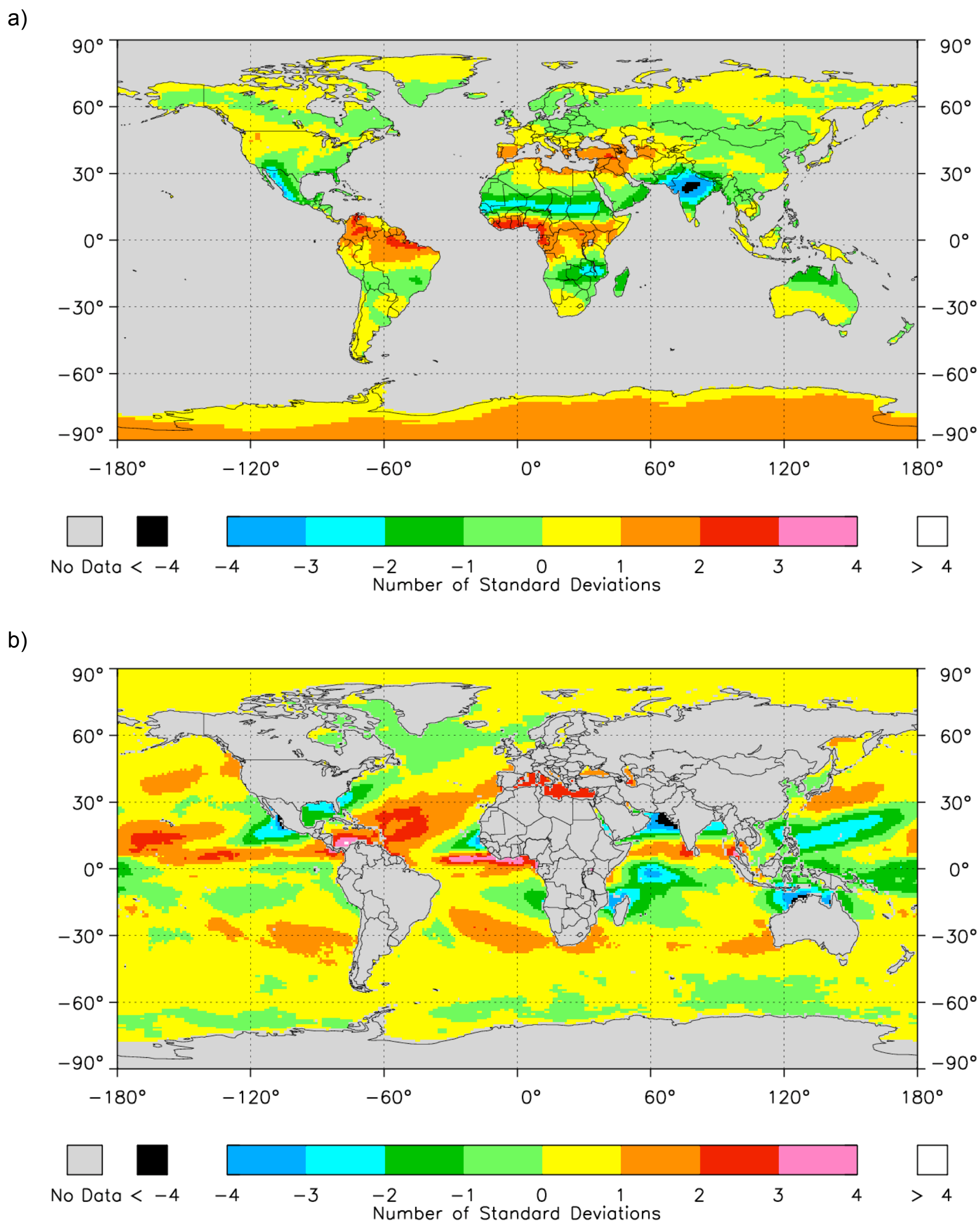

Figure 7. a) EOF-2 of OLR over land and b) EOF-3 of OLR over ocean, representing the semiannual cycle.

a)

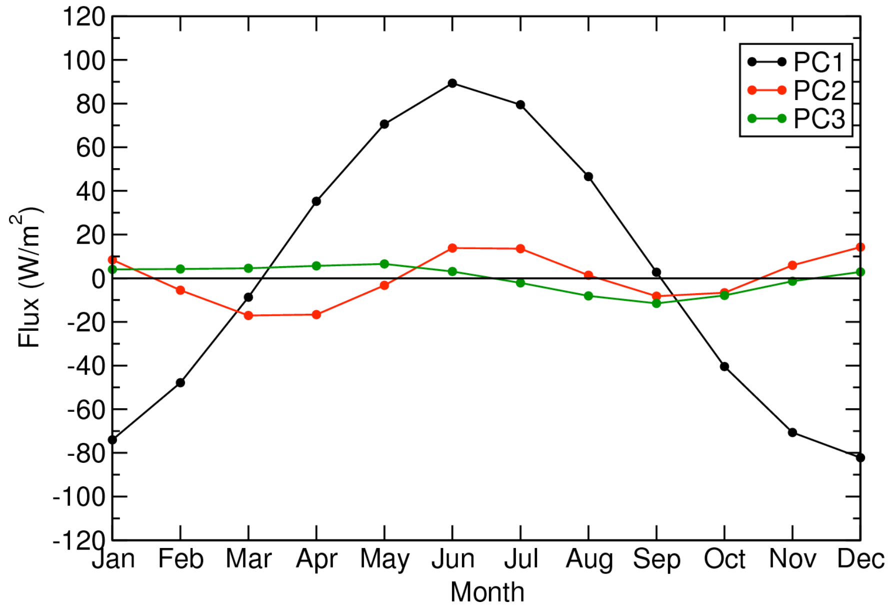

b)

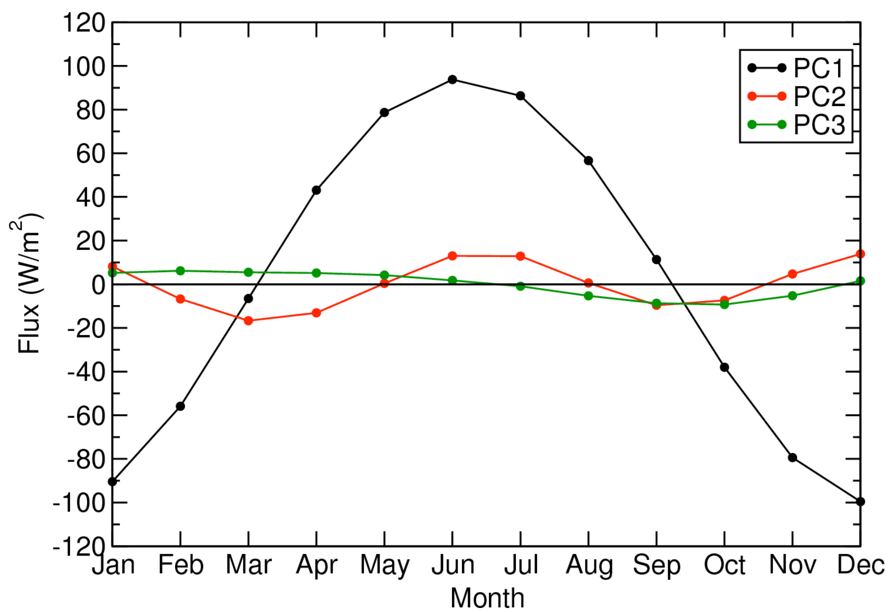

Figure 8. PCs of net radiation over a) land and b) ocean.

a)

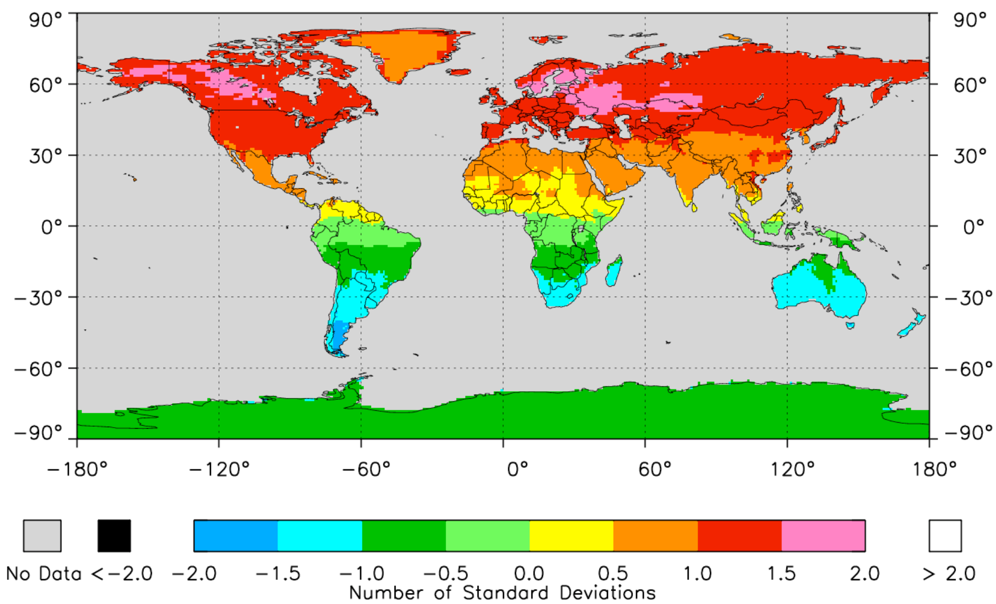

b)

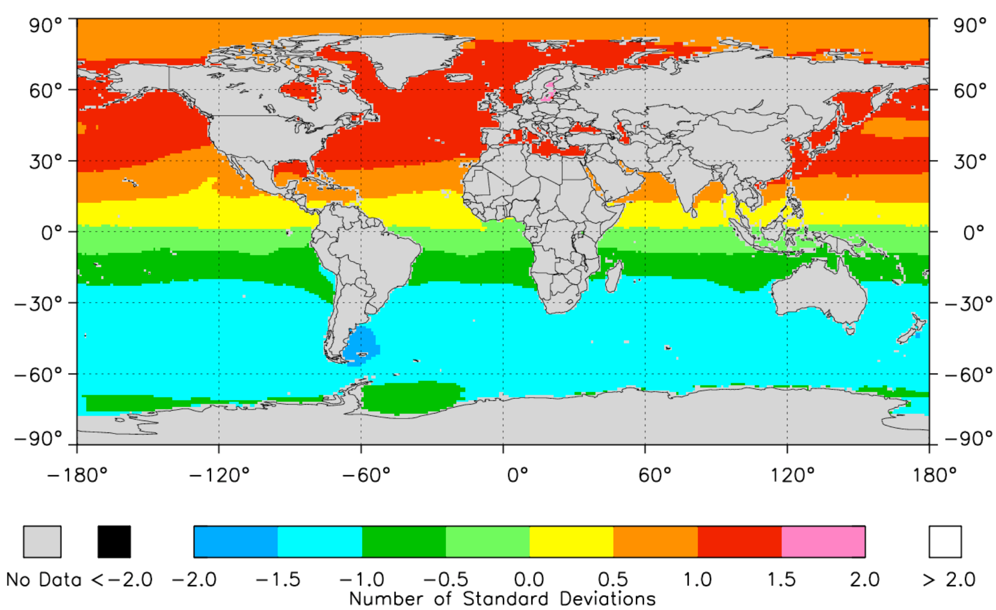

Figure 9. EOF-1 of net radiation over a) land and b) ocean.

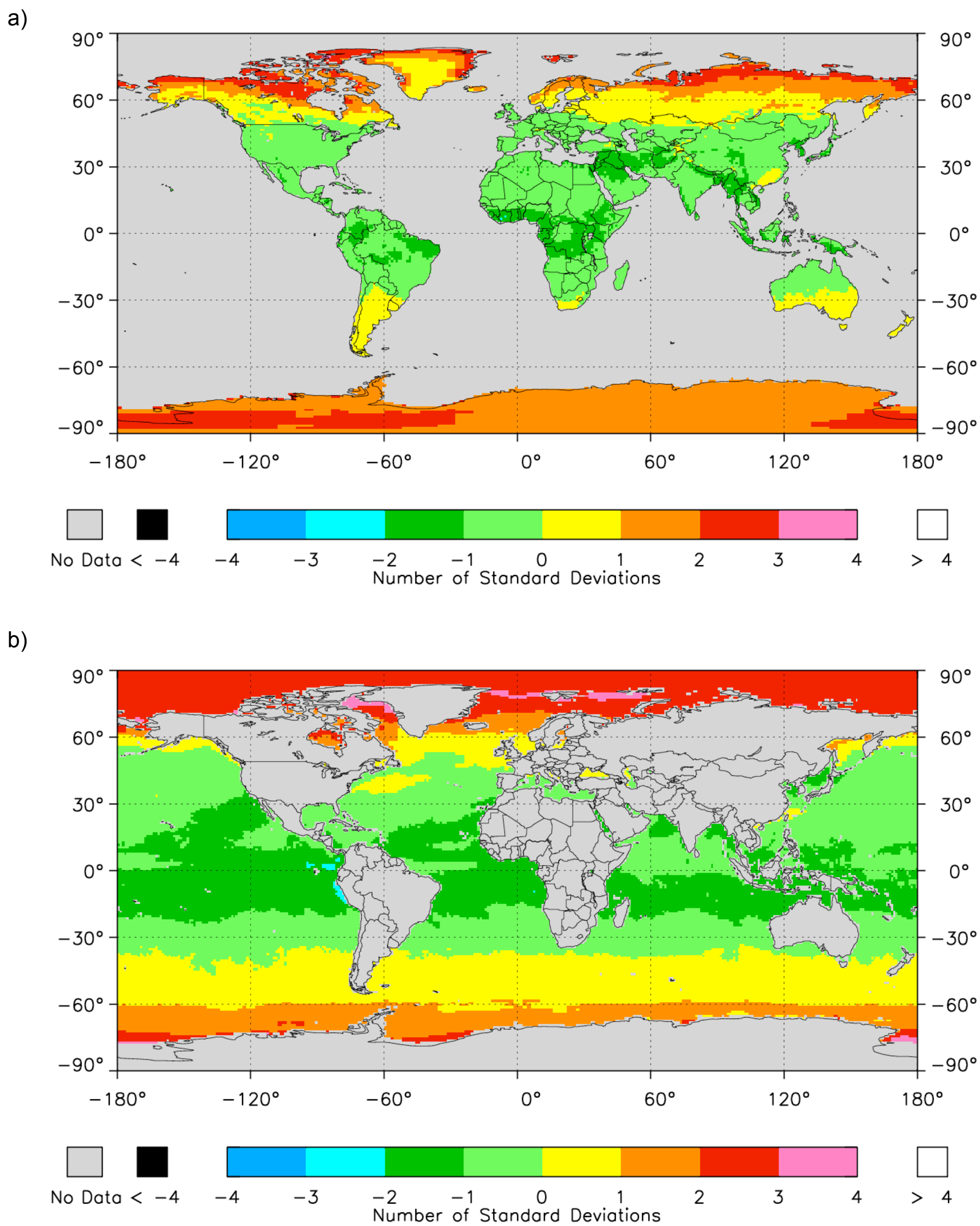

Figure 10. EOF-2 of net radiation over a) land and b) ocean.